Insolation and Greenhouse Gases Drove Holocene Winter and Spring Warming in Arctic Alaska

William M. Longo[a,b,1,*], Yongsong Huang[a,b], James M. Russell[a,b], Carrie Morrill[c,d], William C. Daniels[a,b], Anne E. Giblin[e], Josue Crowther[a]

a) Department of Earth, Environmental and Planetary Sciences, Brown University, 324 Brook Street, Providence, RI 02912

b) Institute at Brown for Environment and Society, Brown University, 324 Brook Street, Providence, RI, 02912, USA

c) Cooperative Institute for Research in Environmental Sciences, University of Colorado Boulder, 216 UCB, Boulder, CO 80309

d) NOAA's National Centers for Environmental Information, Center for Weather and Climate, 325 Broadway, Boulder, CO 80309

e) The Ecosystems Center, Marine Biological Laboratory, 7 MBL Street, Woods Hole, MA 02543

1) *Current Affiliation*: Department of Marine Chemistry and Geochemistry, 266 Woods Hole Road, Woods Oceanographic Institution, Woods Hole, MA 02543, USA

* Corresponding Author:

William M. Longo
email: wlongo@whoi.edu
Tel: +1 508 289 2921

Keywords: Continental biomarkers; Alkenone; Paleoclimatology; Paleolimnology; Temperature reconstruction; Proxy data-model comparison; Holocene; North America; Seasonality; Beringia

Abstract

Global surface temperature changes and their drivers during the Holocene Epoch remain controversial. Syntheses of proxy data indicate that global mean annual temperature declined from the mid-Holocene until the Pre-industrial Era, a trend linked to decreasing Northern Hemisphere summer insolation. In contrast, global climate models simulate increasing mean annual temperatures driven by retreating ice sheets and increasing greenhouse gas concentrations. This proxy-model disagreement may originate from a warm season bias in Northern Hemisphere proxy reconstructions, highlighting the need for new proxies that quantify cold season temperature, especially in Arctic regions that were devoid of continental ice sheets during Holocene. Here, we present a new 16,000-year winter-spring temperature reconstruction derived from the unsaturation ratio of alkenones (U) in a continuous sedimentary sequence from Lake E5, northern Alaska. We employ a thermodynamic lake model to convert alkenone-inferred lake temperatures into winter-spring air temperature anomalies and we contextualize our proxy reconstruction with climate model output from the region. Our reconstruction shows that winter-spring temperatures warmed rapidly during the deglaciation at 16 and 14 thousand years before present and continued to warm gradually throughout the middle and late Holocene (0.12 - 0.28 °C/thousand years) in concert with regional sea surface temperature and sea ice records. Our results are consistent with climate model simulations and we attribute Holocene warming to rising winter-spring insolation, radiative forcing from rising greenhouse gas concentrations and regional feedbacks. Our reconstructed cold season warming equaled or exceeded summer cooling according to a regional synthesis of terrestrial temperature records, suggesting that seasonal biases in temperature reconstructions may account proxy-model disagreements in Holocene temperature trends from Eastern Beringia.

1. Introduction

Global climate models (GCM) simulate increasing mean annual surface temperature during the Holocene, primarily driven by retreating Northern Hemisphere ice sheets in the early Holocene and increasing greenhouse gas (GHG) concentrations after eight thousand years before present (ka cal BP; Liu et al., 2014). In contrast, syntheses of globally distributed continental and marine proxy reconstructions indicate that the mean surface temperature was warm during the early Holocene Climate Optimum (10 – 6 ka cal BP) and subsequently cooled through the Pre-industrial Era (PI; Marcott et al., 2013). This cooling is inferred to result from the large (~40 W m^{-2}) reduction in Northern Hemisphere summer insolation (NHSI), due to changes in Earth's orbital geometry. However, orbital forcing caused increases in southern hemisphere summer insolation over the same interval and no appreciable change in globally and annually averaged incoming solar radiation (Laskar et al., 2004). Thus, reconstructed early Holocene warmth and subsequent cooling could only have been realized through strong global climate feedbacks to NHSI (Marcott et al., 2013), such as reduced albedo from expanded boreal forests (Foley et al., 1994). Other studies have proposed that a bias in climate proxies towards boreal summer accounts for the Holocene cooling trend and data-model mismatch (Liu et al., 2014; Meyer et al., 2015; Baker et al., 2017; Marsicek et al., 2018). For example, the removal of summer-sensitive marine records from North Atlantic margins reduced the data-model difference in the global synthesis, but even after correction the proxy data do not indicate a warming trend (Marsicek et al., 2018), leaving this "Holocene temperature conundrum" unresolved.

Newer paleoclimate records and syntheses have indicated Holocene winter warming, suggesting that better representation of seasonality in paleoclimate reconstructions could partly resolve the proxy data-model disagreement (Meyer et al., 2015; Baker et al., 2017; Marsicek et al., 2018). However, these reconstructions are either limited in duration or predominantly from terrestrial northern mid-latitude regions that are highly sensitive to ice sheet forcing (Clark et al., 1999), making them hard to extrapolate to the global mean. The waning Laurentide Ice Sheet (LIS) was far east of Alaska by the start of the Holocene Epoch (Dyke, 2004) and had a little impact on Holocene temperatures there according to proxy data (Kaufman et al., 2004). Therefore, Alaska is a crucial region for reconstructing seasonally resolved Holocene temperature change in the absence of significant regional ice sheet feedbacks. New cold season temperature reconstructions from such regions are essential for identifying seasonal biases in global proxy data and deconvolving the relative importance of Holocene climate forcing mechanisms and feedbacks.

Despite the importance of Alaskan cold season climate to resolving Holocene temperature trends and forcings, there are few continental temperature records representing the non-summer seasons from the region (Sundqvist et al., 2014). Pollen assemblages have been used to develop winter temperature reconstructions from lake sediments (Viau et al. 2008; Bartlein et al. 2011), however tundra plant species with large geographic ranges result in “non-analog” assemblages preventing accurate winter temperature estimates (Birks et al., 2011). Oxygen isotope analyses of ice wedges have

113 emerged as techniques to provide winter temperature reconstructions (Opel et al., 2018),
114 however these archives have rarely provided continuous whole-Holocene records in the
115 Arctic and are less common or accessible than other continental climate archives. Other
116 moisture-sensitive oxygen isotope records have been used as winter climate indicators
117 through their sensitivity to the strength and position of the Aleutian Low (e.g. Anderson
118 et al., 2005; Clegg et al., 2010). However, interpretations of these records remain
119 complex (Kaufman et al., 2016) and none of these records directly record temperature
120 changes.
121
122 In this study, we generate a new winter-spring temperature reconstruction from Arctic
123 Alaska using sediment cores from Lake E5 (68.642 °N, 149.458 °W, 798 m a.s.l.). To
124 reconstruct winter-spring temperatures, we utilize alkenones – a series of biomarkers
125 produced by various species of haptophyte algae (Volkman et al., 1980; Marlowe et al.,
126 1984; D'Andrea et al., 2006) occurring globally in oceans (Conte et al., 2006) and in
127 many freshwater lakes (Longo et al., 2018). Our recent work demonstrates that Lake E5
128 alkenones are produced by the freshwater-dwelling clade of alkenone-producing
129 Isochrysidales haptophytes (Richter et al., 2019), during the spring transitional season
130 (Longo et al., 2016; 2018; Richter et al., 2019). The degree of unsaturation of 37-carbon
131 alkenones records spring lake temperature with high precision (±1.37 °C) by way of the
132 U index (Brassell et al., 1986) and our site-specific U temperature calibration (Longo et
133 al., 2016). Lake temperature and lake ice phenology in the spring are controlled by winter
134 and spring air temperatures due to the high thermal inertia of lakes and their accumulated
135 winter ice cover (Palecki and Barry, 1986; Assel and Robertson, 1995; Livingstone,

1997; Magnuson et al., 2000; Arp et al., 2013). Accordingly, the alkenone proxy responds strongly to winter lake ice conditions and correlates with air temperatures of the late winter and spring in many freshwater lakes (Longo et al., 2018).

We carried out a series of modeling experiments by forcing a one-dimensional thermodynamic lake model (Hostetler and Bartlein, 1990) calibrated to our study site, with a series of Holocene climate simulations from the Proxy Model Intercomparison Project Phase III (PMIP3; Braconnot et al., 2012). Results from these experiments support the interpretation that alkenones record winter-spring air temperature changes and they quantify the lake temperature-air temperature relationship at Lake E5. We combine our novel winter-spring temperature reconstruction with PMIP3 and transient climate model output from the region to elucidate Holocene winter-spring temperature evolution in Arctic Alaska and identify forcing mechanisms driving Holocene temperature trends.

2. Regional Setting

The North Slope of Alaska lies between 68°N and 71°N and comprises three physiographic regions—the Brooks Range Mountains, Arctic Foothills and Arctic Coastal Plain—that are situated south to north along a gradient of decreasing temperature and elevation (Hobbie and Huryn, 2012). Lake E5 is a kettle lake (Surface Area = 0.109 km^2; Maximum Depth = 12.7 m; Mean Depth = 6.33 m) situated in the Arctic foothills on an upland tundra landscape underlain by continuous permafrost (Fig. 1). The catchment was free of glaciers throughout the last glacial period (Hamilton, 1982) and the lake underwent continuous sedimentation dating to 32 ka cal BP offering a rare uninterrupted record of the Last Glacial Maximum (LGM), deglaciation, and Holocene (Eisner and Colinvaux, 1992; Vachula et al., 2019). Lake E5 is oligotrophic and ice-free from mid-June through late September. Mean annual air temperatures at Lake E5 are -8 °C with low winter temperatures of -35 °C and high summer temperatures of 20 °C (Hobbie and Huryn, 2013). Mean annual precipitation for the region is 292 mm yr^{-1} and mean annual evapotranspiration is 127 mm yr^{-1} (Dery et al., 2005).

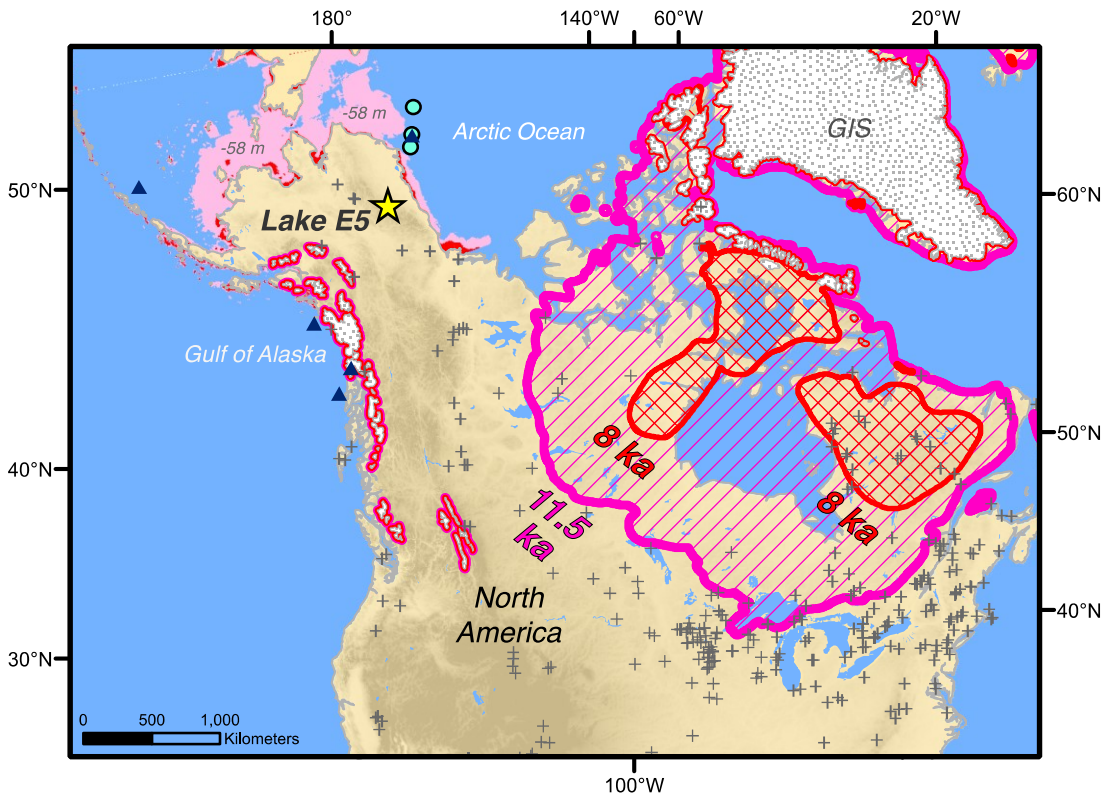

Fig. 1. Study site and early Holocene ice sheet extent. Map of North America showing the extent of the LIS at 11.5 ka cal BP (magenta hatch) and 8 ka cal BP (red cross-hatch; Dyke et al., 2004), and estimated extent of exposed shelf surrounding Alaska at 11.5 ka cal BP (pink shading) and 8 ka cal BP (red shading; Manley et al., 2002), respectively. Lake E5 is marked with the yellow star. "GIS" refers to the Greenland Ice Sheet. Records used in the recent pollen synthesis ("+" symbols; Marsicek et al., 2018) are dominated by mid-latitude sites. Sea surface temperature (navy triangles) and sea-ice (teal circles) reconstructions discussed in the text are indicated.

3. Materials and Methods

3.1. Sediment Core Retrieval, Processing and Chronology

Sediment cores were collected from the deepest part of Lakes E5 in May, 2014 over ~1 m of lake ice cover, using a piston corer for surface cores and a modified Livingstone corer for subsequent cores. Six vertical meters of sediment were collected, the top 4.8 m of which resulted in a continuous sedimentary record. Cores were returned to Brown University, logged visually, and were imaged and logged for Magnetic Susceptibility and X-ray Fluorescence using a Geo-Tek™ multi-sensor core logger. Overlapping cores were aligned based on visually distinct beds and lithological parameters including organic carbon content, magnetic susceptibility, and elemental data. Aligned cores were spliced to create a continuous 4.8 m sedimentary sequence.

1-2 cm thick samples were aliquoted and frozen for radiocarbon dating from the working halves of split and logged cores. For radiocarbon processing, ~ 5 cm^3 subsamples were sieved at 500 and 150 μm. From the sieved fractions, terrestrial plant and insect macrofossils were collected under a dissecting microscope, characterized, and treated for ultra-microscale radiocarbon analysis (Shah Walter et al., 2015). The full radiocarbon and ^{210}Pb chronology is published by Vachula et al. (2019; Fig. S1) and consists of 16 radiocarbon dates and ^{210}Pb dating in the uppermost sediments. Holocene aged sediments consist of brown thickly bedded silts, deglacial sediments consist of black and green laminated silts and clayey silts.

199 *3.2. Alkenone Analysis and U Temperature Determinations*

200

201 Alkenone analysis was carried out using established methods (Longo et al., 2016).
202 Sediment cores were sampled in 1 cm sections and samples were freeze-dried,
203 homogenized and extracted using an accelerated solvent extraction system (ASE200;
204 Dionex). Neutral lipids were separated from fatty acids by flash column chromatography
205 using Supelco™ Supelclean LC-NH2 powder. A ketone fraction was eluted from the
206 neutral lipids with dichloromethane by way of flash column chromatography with silica
207 gel. Ketone fractions were saponified before analysis by GC-MS to check peak purity and
208 further analyzed by GC-FID for quantification.

209

210 GC-MS analysis was performed using an Agilent 6890N GC system coupled to an
211 Agilent 5973N quadrupole mass spectrometer and GC-FID analysis was performed
212 using an Agilent 7890B GC system with the operating conditions outlined by Longo et al.
213 (2016). All GC-MS and GC-FID analyses were performed with a VF-200ms 60m
214 capillary column, allowing for full separation of Group I alkenone distributions (Longo et
215 al., 2013). Alkenone quantification was accomplished using 18-pentatriacontanone as an
216 internal standard and all injections were made within a narrow dynamic range of ~2-20
217 ng of C_{37} alkenones on column to reduce analytical uncertainties in alkenone
218 quantification. Analytical error on U-inferred temperatures is ± 0.20 °C (1SD) based on
219 replicate analyses of alkenone standards and sediment core samples. The uncertainty in
220 the temperature calibration (± 1.37 °C) includes this analytical error (Longo et al., 2016).

221

222 *3.3. Proxy Fundamentals and Interpretation*

223

224 Alkenones in Lake E5 and nearby Toolik Lake (68.632 °N, 149.602 °W) are produced by
225 the Group I phylotype of Isochrysidales haptophyte algae, which is the dominant group in
226 freshwater environments (Longo et al., 2016; 2018; Richter et al., 2019). The relationship
227 between Group I alkenone unsaturation and temperature is broadly consistent across sites
228 in the Northern Hemisphere (D'Andrea et al., 2011; 2016; Longo et al., 2016; 2018) and
229 has been robustly quantified at Toolik Lake (Longo et al., 2016). An in situ calibration
230 from Lake E5 indicates that Lake E5 and Toolik Lake calibrations are statistically
231 indistinguishable (Fig. S2). Therefore, the published Toolik Lake calibration (Longo et
232 al., 2016) is used for lake water temperature determinations.

233

234 Group I Isochrysidales haptophytes are most abundant in the water column of Lake E5
235 and its neighboring lakes in the spring, during the periods of partial ice cover, isothermal
236 spring mixing, and at the onset of thermal stratification (Richter et al., 2019). We
237 collectively refer to these periods, which occur during the month of June at Lake E5, as
238 the spring transitional season. Geochemical and observational data have shown that
239 alkenone production and deposition occur during this spring transitional season, which is
240 characterized by lake surface temperatures ranging from 2 to 15 °C (Longo et al., 2016;
241 2018). These springtime sedimentary fluxes of Group I alkenones are also seen in
242 Norway (D'Andrea et al., 2016), whereas southwest Greenland lakes show a slightly later
243 peak flux, shortly after ice out (D'Andrea et al., 2011).

244

245 Spring lake temperatures and lake ice break-up are dominantly influenced by the mean
246 temperature of the preceding 1-6 months, through the effects of winter and early spring
247 temperature on lake ice accumulation and the timing of spring thaw (Palecki and Barry,
248 1986; Robertson et al., 1992; Assel and Roberston, 1995; Livingstone, 1997; Magnuson
249 et al., 2000; Arp et al., 2013). Accordingly, alkenone unsaturation has been shown to
250 correlate with late winter and spring air temperature (Longo et al., 2018). Additionally,
251 surface sediment and sediment trap data from Toolik Lake with accompanying year-
252 round lake ice phenology data, corroborate the interpretation of the proxy as reflecting
253 winter-spring climate, with colder U–inferred lake temperatures corresponding with
254 longer ice-out periods and later ice-off dates (Fig. S3; Toolik Environmental Data Center
255 Team, 2016). Within our proxy framework, these data suggest that colder temperatures in
256 the winter and spring, which result in more ice accumulation on the lake surface, have
257 lasting effects on spring lake temperature through the thermodynamic requirement of
258 melting a thicker ice cover and the delaying of summer lake surface warming through
259 extended ice cover. The Group I haptophytes have a consistent spring bloom timing and
260 therefore record spring lake temperatures dominated by these seasonal lake ice dynamics.
261
262 Changes in alkenone-producing haptophyte species have been known to overprint
263 alkenone-inferred temperatures in lakes (Randlett et al., 2014). The RIK_{37} index (Longo
264 et al., 2016) was calculated for all samples to evaluate species effects, which were absent
265 from the record (Fig. S4).
266
267

3.4. Lake Model Description, Parameterization and Validation

The Hostetler and Bartlein lake model is a one-dimensional energy- and water-balance model that requires inputs for near-surface air temperature, humidity, wind speed, surface incident shortwave and longwave radiation, surface pressure, precipitation, and runoff (Hostetler and Bartlein, 1990, Dee et al., 2018). Meteorological inputs from 1994 – 2015 CE were obtained from the Toolik Environmental Data Center (5 m air temperature, 5 m relative humidity, 5 m wind speed, surface incident shortwave radiation, surface air pressure; Toolik Environmental Data Center Team, 2016) and from the Imnaviat Creek Snotel site (precipitation; SNOTEL, site 968). Toolik Lake is approximately 5 km west of Lake E5 and the Imnaviat Creek site is approximately 7 km east of Lake E5. Downward longwave radiation values are available only for the end of the record (May 2013-December 2014). To extend longwave values back to 1994, a multiple linear regression relationship between this variable, air temperature, and relative humidity was calculated for the 19-month period when all three variables were measured. Toolik EDC meteorological data are hourly and the Snotel data are daily. For missing values in the meterological dataset, data gaps less than or equal to six hours in duration were filled using linear interpolation. Daily precipitation amounts were divided evenly across the 24-hour period and missing values for precipitation were set to zero.

A series of present-day simulations were used to determine the most appropriate values for several adjustable lake-specific parameters in the lake model. To carry out these simulations, the model was run with a 10-year spin-up period using repeated 2008 data,

291 followed by the 21-year meteorological dataset. The lake-specific parameters include the
292 neutral drag coefficient, the albedos of snow and melting snow, and the shortwave
293 extinction coefficient. These parameters were calibrated by comparing lake model output
294 from 2008-2014 CE to limnological data obtained from both the Toolik Environmental
295 Data Center (Toolik Environmental Data Center Team, 2016) and the Arctic Long Term
296 Ecological Research program (ARC LTER database; NSF-DEB-1637459), including
297 mean lake temperature, maximum summer lake temperature, break-up date, freeze-up
298 date, and mixing depth. The 2008-2014 CE period was selected for validation because of
299 its comprehensive data coverage in both meteorological data and limnological data.
300 Sensitivity tests indicated that the neutral drag coefficient and albedo terms had the
301 greatest effects on modeled lake temperatures. The neutral drag coefficient was set to
302 0.002 and the albedos of slush and snow were set to 0.4 and 0.7, respectively. Lake size
303 had only minimal effects (< 0.3 °C difference in average spring lake temperature between
304 Lake E5 and Toolik Lake-sized basins). The fully calibrated lake model was then
305 employed for Lake E5 6 ka experiments.
306
307 For visualization of model performance, lake model output at 1.5 m depth was compared
308 with measured lake temperature at 1 – 2.2 m depth, and seasonal ice cover at Toolik Lake
309 (Fig. S5). Observed lake temperature is derived from a fixed sensor in the lake therefore
310 its depth varies between 1 and 2.2 m with lake level fluctuations (Toolik Environmental
311 Data Center Team, 2016).
312
313

3.5. GCM Output and Mid-Holocene Lake Model Simulations

GCM outputs from PMIP3 (Braconnot et al., 2012) and three transient simulations – CCSM3 (Liu et al., 2009), LOVECLIM (Timm and Timmermann, 2007), and FAMOUS (Smith and Gregory, 2012; Liu et al., 2014) – were extracted from the four gridcells most proximal to Toolik Lake and Lake E5. 6 ka vs. Pre-Industrial (PI) anomalies were calculated from PMIP3 simulations using the 6 ka and PI outputs. 6 ka vs. Present-Day (PD) anomalies were calculated using the PMIP3 6 ka outputs and modern outputs (1981-2005 CE) from CMIP5 historical simulations. For the transient simulations, anomalies were calculated as the average temperature from 7 – 5 ka cal BP minus the average temperature at 1750 – 1850 CE. The same PI reference period (1750-1850 CE) was applied to calculate alkenone-derived air temperature anomalies.

Mid-Holocene (6 ka) lake model simulations were carried out using climatology outputs from eight GCMs participating in PMIP3 (Braconnot et al., 2012) with the necessary variables for the lake model (BCC-CSM1-1, CCSM4, CNRM-CM5, GISS-E2-R, HadGEM2-ES, IPSL-CM5A-LR, MIROC-ESM, MRI-CGCM3). 6 ka input datasets for the lake model were developed by applying the change in climatology between 6 ka and PD simulated by each PMIP3 model to the modern meteorological (control) inputs. This approach alleviates issues with biases in climate model output for present-day climate, although biases can still impact the magnitude of the modeled change between 6 ka and PD. To generate climatologies, at least 100 years of GCM output was averaged for the 6 ka time period, and 75 years of GCM output (1981-2005 CE for three ensemble

337 members) was averaged for the PD from the CMIP5 historical simulations. For most of
338 the meteorological variables, the percentage change between the modern and 6 ka
339 simulations was used to scale the observational data for input to the lake model. For air
340 temperature, the only variable that can have negative values, the temperature anomaly
341 was directly applied to the modern dataset. Likewise, the anomalous wind speed change
342 for the MIROC-ESM and IPSL-CM5A-LR models was directly applied given their small
343 (<2 m/s) climatological values for this variable that yield unrealistically large percentage
344 changes between the 6 ka and PD time periods. Given the dependence of relative
345 humidity on temperature, this variable was scaled by first converting to specific humidity
346 and applying the modeled percentage change in specific humidity, then converting back
347 to relative humidity using the anomalous temperature value.
348
349 Each 6 ka lake model simulation was first spun up for 10 years to reach equilibrium as
350 defined by stabilization of lake temperature, and then run over the 21-year meteorological
351 period, ensuring that a full range of inter-annual climate variability was captured in the
352 simulations.
353
354 *3.6. Simulated Spring Lake Temperature vs. Winter-Spring Air Temperature*
355
356 For comparison to the alkenone proxy, the average spring lake temperature was extracted
357 from model outputs as the averaged epilimnion + metalimnion temperature 30 days
358 before and after the average ice-off date. These criteria were chosen based on
359 observations of alkenones in Lake E5 and Toolik Lake (Longo et al., 2016; 2018). The

360 regression of this simulated spring lake temperature vs. DJFMAM air temperature from
361 several 6 ka lake model simulations was used to transform proxy-derived spring lake
362 temperature estimates into DJFMAM air temperatures (Fig. 2). Each point in the ordinary
363 least squares regression represents a lake model simulation forced by a single 6 ka
364 climate model input (abbreviated, respectively, from above: BCC, CCSM, CNRM, GISS,
365 HADGEM, IPSL, MIROC, MRI), the ensemble mean, or the control run with modern
366 meteorological data. Outputs produced by CCSM were not included in the regression
367 because they produced anomalously cold lake temperatures due to anomalously cold June
368 air temperatures relative to the other ensemble members (-3SD from the ensemble mean).
369 These cold June temperatures prevented stratification in the early summer and thus
370 caused a lake stratification regime shift in the lake model, making the resulting spring
371 lake temperatures incomparable with the other simulations. The MIROC output was also
372 excluded from the regressions because it produced anomalously warm spring lake
373 temperatures relative to other simulations and forced the regression to inadequately fit the
374 control simulation. (Exclusion of MIROC resulted in only minor changes in the
375 regression slopes; Fig. S6).
376
377 Regressions demonstrate that spring lake temperature and ice-off date are strongly
378 correlated with winter-spring (DJFMAM) air temperature (Figs. 2, S6). We used the
379 regression to transform reconstructed spring lake temperatures at Lake E5 into DJFMAM
380 air temperature estimates, which are displayed as anomalies relative to pre-industrial (PI;
381 Fig. S7). The transfer function assumes that the regression slope is stationary throughout
382 the Holocene. We suggest this assumption is reasonable given the relatively small range

in spring lake temperature change over this period, however a formal test of this assumption is not possible with the available climate model output.

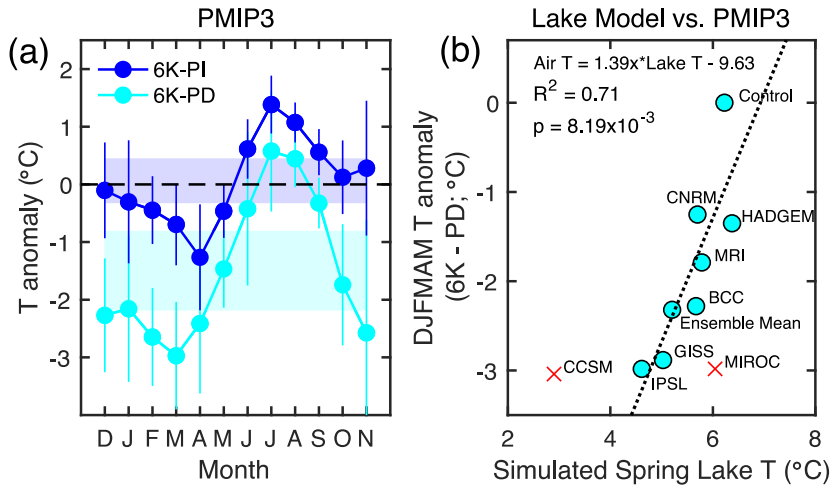

Fig. 2. Simulated mid-Holocene temperatures at Lake E5. (a) PMIP3 ensemble mean surface air temperatures at Lake E5 at 6 ka relative to the PI (pre-industrial) and PD (present day), shown as monthly (points) and mean annual (shaded regions) anomalies. (b) The linear regression of lake model simulated spring lake temperature at 6 ka with PMIP3 simulated winter-spring air temperature anomalies at 6 ka relative to the PD. Points are labeled by the PMIP3 output (ensemble mean or individual models) used to drive lake model simulations. The simulation labeled "control" was forced with the modern meteorological data. Two outlying simulations are marked with a red "x" and discussed in the text.

3.7. Statistical Analyses

Temperature trends for Holocene time series intervals (11.7 ka cal BP – PI and 8 ka cal BP – PI) were determined using ordinary least squares regression and their significance was assessed using an F-test. To incorporate the uncertainties of the U temperature determinations into our analysis of temperature trends, we carried out Monte Carlo simulations. The experiments simulate 1,000 realizations of the alkenone time series drawn at random given the 1SD uncertainty of ± 1.37 °C. Ordinary least squares

404 regressions were carried out for each of the 1,000 simulations and the SD of the resulting
405 regression coefficients is used to provide a comprehensive estimate of the uncertainty in
406 temperature trends. The same Monte Carlo experiments were used to determine the
407 uncertainty of reported mean temperatures over discrete intervals (e.g. Early Holocene, 8
408 – 6 ka cal BP cold period, etc.) and spring lake temperature changes (ΔT) associated with
409 warming events. The statistical significance of rapid warming events was checked using
410 paired, two-tailed T-tests. All uncertainties are reported as ± 1SD unless noted otherwise.

411 **4. Results and Discussion**

412 *4.1. Rapid Deglacial Warming of Spring Lake Temperatures*

413

414 Alkenones appear in the Lake E5 record at 16.2 ka cal BP and indicate three stages of
415 rapid deglacial warming (Fig. 3). The first warming, from 16.2 – 15.5 ka cal BP
416 represents a ~2 °C increase in lake temperature and coincides with regional climate
417 changes including the second phase of alpine glacial retreat in the Brooks Range
418 (Pendleton et al., 2015) and warming in Northwestern Alaska (Kurek et al., 2009). The
419 second warming stage of 2.2 ± 0.5 °C occurred from 14.5 – 13.7 ka cal BP, culminating
420 in the most rapid and sustained temperature increase in the record. This major warming
421 event is associated with contemporaneous records of vegetation change, soil development
422 and thermal degradation of permafrost from the region (Anderson and Brubaker, 1994;
423 Mann et al., 2002; 2010; Abbott et al., 2010). Temperatures then warmed again from 12.0
424 – 11.6 ka cal BP by ~1 °C, marking the onset of Holocene climate (Fig. 3).

425

426 Spring lake temperatures at Lake E5 prior to 14.5 ka cal BP averaged 4.00 ± 1.49 °C and
427 were accompanied by the highest C_{37} alkenone concentrations in the record (Figs. 3, S4).
428 These data are consistent with prolonged springtime alkenone production during a cold
429 polymictic stratification regime. We infer a dimictic stratification regime for spring lake
430 temperatures above 5 °C based on modern observations that Lake E5 begins to thermally
431 stratify in the spring when lake temperatures reach 5 – 6 °C (ARC LTER database).
432 Therefore, the prominent warming event from 14.5 – 13.7 ka cal BP likely caused a shift
433 in Lake E5's stratification regime.

The 14.5 – 13.7 ka cal BP warming in our record corresponds with the Bølling-Allerød winter warming reconstructed from ice wedge oxygen isotopes at Barrow in coastal north-central Alaska (Meyer et al., 2010). Ice wedges derive from winter precipitation and therefore their $\delta^{18}O$ signatures reflect winter climate and primarily, winter temperature (Meyer et al., 2010; Opel et al., 2018). Our record corroborates findings by Meyer et al. (2010) that the maximal Bølling-Allerød winter warming in the region lagged warming in Greenland by ~1 ka. However, the records diverge during the Younger Dryas (YD), as Lake E5 alkenones do not record the severe winter cooling indicated by the Barrow Ice Wedge System (Meyer et al., 2010). This also contrasts with records from the North Atlantic where YD cooling is thought to be enhanced during winter due to strong sea-ice feedbacks (Denton et al., 2005). The YD is only seen sporadically in terrestrial records from the region (Kokorowski et al., 2008), but is recorded prominently in north-central Alaskan paleoecological records (Mann et al., 2002; 2010) and temperature reconstructions (Meyer et al., 2010; Gaglioti et al., 2017).

Younger Dryas climate impacts are likely spatially complex in northern Alaska due to sea ice export from the Chukchi and Beaufort Seas driven by Bering Strait resubmergence and deglacial sea level rise (Bradley et al., 2008). Therefore, one potential explanation for the lack of correspondence between YD temperatures reconstructed at Lake E5 vs. records from Barrow and North-central Alaska could be regional heterogeneities in the feedbacks and mitigating factors that determined the magnitude of YD cooling. We must also consider the possibility that the YD signal at Lake E5 was dampened or modified by

457 aforementioned changes in the stratification regime that occurred around this time.
458 Despite this lack of regional correspondence in YD cooling, deglacial warming events at
459 Lake E5 align well with several other temperature, hydrological and paleoecological
460 reconstructions (e.g. Abbott et al., 2010; Mann et al., 2010; Meyer et al., 2010; Pendleton
461 et al., 2015) lending support to our reconstructed deglacial lake temperatures.
462
463 *4.2. Holocene Winter-Spring Temperature and Comparison with GCMs*
464
465 Gradual warming dominates the Holocene spring lake temperature trend in our record
466 (11.7 ka cal BP – PI; 0.087 °C/ka; $p = 1.12 \times 10^{-3}$). The early to mid-Holocene transition
467 (EMHT) at 8 ka cal BP, marked the collapse of the LIS and Earth's full transition to post-
468 glacial boundary conditions (Stager and Mayewski, 1997), therefore we also consider the
469 warming trend that began during this event and persisted throughout the middle and Late
470 Holocene (8 ka cal BP – PI; 0.20 °C/ka; $p = 6.35 \times 10^{-5}$). The post-EMHT amplitude of
471 warming exceeds the Holocene average owing to a local temperature minimum at ~7 ka
472 cal BP driven, in part, by multi-centennial variability. Both trends are robust after
473 accounting for the uncertainty in U temperature determinations (Fig. 3; Table S3).
474

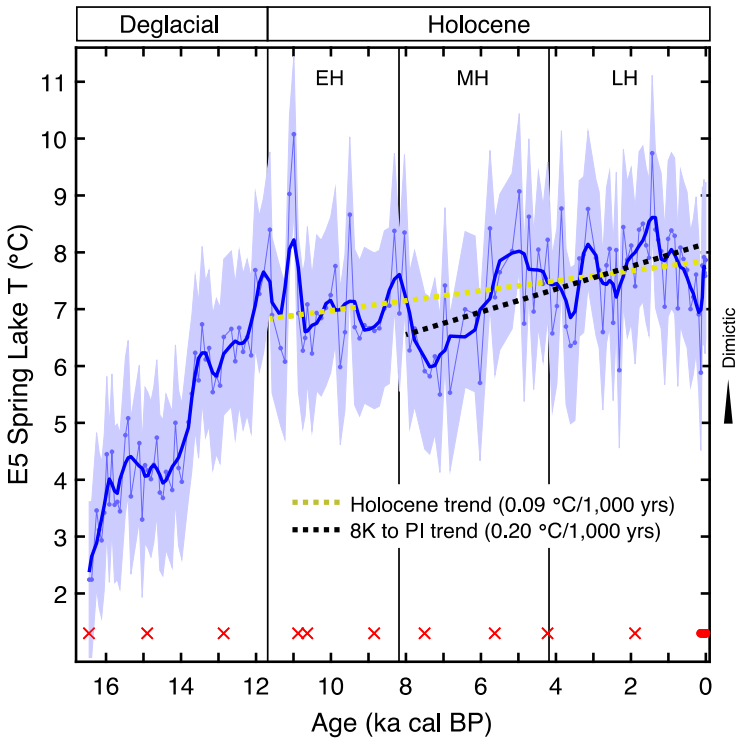

Fig. 3. 16,000-year record of spring lake temperature from Lake E5. The data is overlaid with a smoothing function (LOWESS; span = 7; α = 0.05) and the uncertainty in the reconstruction is plotted as the light blue error envelope (±1SD). Statistically significant warming trends are shown for the whole Holocene (yellow dashed line) and 8 ka cal BP – PI (black dashed line). Age control points are plotted in red along the bottom ("X" indicates ^{14}C and "o" indicates ^{210}Pb). EH, MH and LH refer to the early, middle and late Holocene, respectively. A dimictic stratification regime is inferred for spring lake temperatures above 5 °C based on modern observations.

Spring lake temperatures scale linearly with winter-spring air temperature according to our 6 ka lake model simulations, and are suppressed relative to air temperature changes. (Fig. 2). We used this relationship to estimate Holocene cold season air temperature and find that the warming trends are 0.12 °C/ka (11.7 ka cal BP – PI) and 0.28 °C/ka (8 ka cal BP – PI). Thus, we estimate that cold season air temperatures warmed by 1.4 °C over the whole Holocene and warmed by 2.2 °C after the EMHT. Although the post-EMHT warming trend may be enhanced by stochastic, high-frequency variability, the pattern of

492 change is conserved after smoothing the record (Fig. S7), suggesting the acceleration of
493 warming in the mid- to late Holocene is a robust feature of the reconstruction.
494
495 The magnitudes and rates of reconstructed winter-spring temperature change at Lake E5
496 are in general agreement with GCM simulations. An ensemble of GCM output from the
497 Proxy Model Intercomparison Project Phase III (PMIP3; Braconnot et al., 2012)
498 simulates 0.5 °C cooler winter and spring temperatures at 6 ka relative to the PI at Lake
499 E5 (Fig. 4), in accordance with the reconstructed temperature minimum at 8 – 6 ka cal BP
500 (Fig. 3). Furthermore, the transient simulation by the Loch-Vecode-Ecbilt-Clio-Agism
501 Model (LOVECLIM, Timm and Timmermann, 2007) simulates moderately warm early
502 Holocene temperatures at Lake E5 followed by a temperature minimum at 7.1 ka cal BP
503 and subsequent warming (Fig. 4). The transient simulation from Community Climate
504 System Model 3 (CCSM3; Liu et al., 2009) reproduces the mild early Holocene
505 temperatures seen in LOVECLIM and the proxy data, however it also simulates a subtle
506 mid- to late Holocene cooling trend (Fig. 4). A transient simulation from the Fast Met.
507 Office and UK universities Simulator (FAMOUS; Smith and Gregory, 2012) indicates
508 pronounced Holocene warming occurring over both intervals in question (11.7 ka cal BP
509 – PI and 8 ka cal BP – PI; Fig. 4). LOVECLIM, the transient ensemble mean (including
510 LOVECLIM, CCSM3 and FAMOUS) and FAMOUS simulate warming trends of 0.064,
511 0.10 and 0.31 °C/ka, respectively, from 8 ka cal BP to the PI (Fig. 4; Table 1). Our
512 reconstructed warming of 0.28 °C/ka falls within this range of GCM estimates.
513 Furthermore, the whole Holocene trend derived from proxy data (0.12 °C/ka) is similar to
514 the transient ensemble mean (0.10 °C/ka) for the same interval (Figure 4; Table 1).

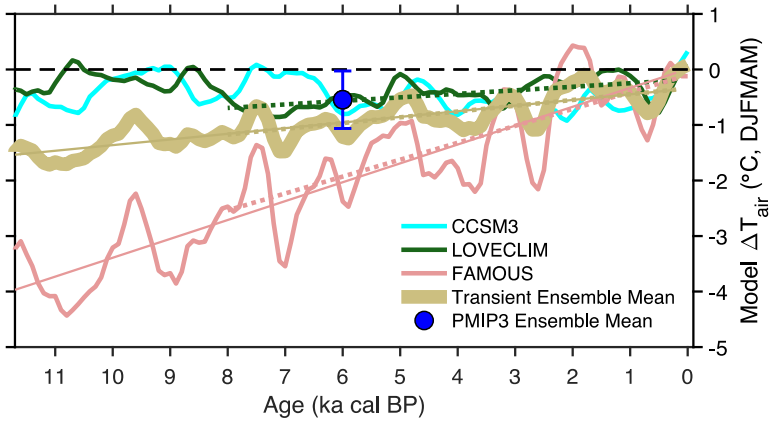

Fig. 4. PMIP3 and Transient simulations of winter-spring air temperature anomalies (vs. PI) at Lake E5. The PMIP3 Ensemble Mean is the average of the 8 simulations used in lake model experiments. The Transient Ensemble Mean is the average of CCSM3, LOVECLIM, and FAMOUS simulations. All transient simulations were resampled and smoothed for comparison with the Lake E5 reconstruction. All significant ($p < 0.01$) post-EMHT warming trends are show with dashed lines. Significant ($p < 0.01$) warming trends over the entire Holocene are shown with solid lines.

Table 1. Summary of Holocene winter-spring temperature trends in proxy data and models.

Time Series	11.7 ka – PI	8 ka – PI
Alkenone-inferred (Spring Lake T, °C/ka)	0.087	0.20
Alkenone-inferred (DJFMAM Air T, °C/ka)	0.12	0.28
LOVECLIM (DJFMAM Air T, °C/ka)	NT	0.064
CCSM3 (DJFMAM Air T, °C/ka)	-0.025	-0.049
FAMOUS (DJFMAM Air T, °C/ka)	0.34	0.31
Transient Ensemble Mean (DJFMAM Air T, °C/ka)	0.10	0.11

NT = no significant trend
All indicated numeric trends are significant ($p < 0.01$)
Positive (negative) trends indicate Holocene warming (cooling)

4.3. Insolation and Greenhouse Gas Forcing of Holocene Winter-Spring Temperature

The distinct structure of Holocene warming recorded at Lake E5 diverges from other cold season temperature reconstructions in Eurasia and North America (Meyer et al., 2015; Baker et al., 2017; Marsicek et al., 2018), and may therefore offer new insight into Arctic cold season climate forcing mechanisms (Fig. 5). The temperature minimum from 8 – 6 ka cal BP at Lake E5 is not observed in these other cold season records (Baker et al., 2017; Marsicek et al., 2018). Notably, it occurs during Holocene minima in winter-spring (DJFMAM) insolation and GHG radiative forcing. These forcings increase by approximately 3.5 W m^{-2} and 0.5 W m^{-2}, respectively, from 8 ka cal BP to the PI and are accompanied by progressive cold season warming at Lake E5. Insolation during the opposite half year (JJASON) provides a much stronger and opposite forcing (-15 W m^{-2}), which is doubled when considering summer insolation alone (JJA; -36 W m^{-2}). Despite its larger amplitude, NHSI did not trigger Holocene cold season cooling according to our reconstruction and GCM simulations.

In addition to orbital and GHG forcing, ice sheet retreat has been identified as a major driver of winter warming during the Holocene in North America, Eurasia, and the North Atlantic (Liu et al., 2014; Baker et al., 2017; Marsicek et al., 2018). Our new reconstruction deviates from these records in the early Holocene, revealing a spatially variable imprint of ice sheet forcing on Holocene cold season climate. At Lake E5, the slightly warmer winter-spring temperatures in the early Holocene (as compared with 8 – 6 ka cal BP) are consistent with a reduced LIS that had retreated into present day north-

554 central and northeastern Canada, more than 1,000 km east of Lake E5 (Fig. 1, Dyke et al.,
555 2004). We observe periods of warmth and even a slight cooling as retreat continued
556 during the early Holocene, indicating that ice sheet effects were minimal or non-existent
557 at our site (Fig. 5). In contrast, a recent synthesis of pollen records from North America
558 and Europe shows cold season warming from the early to mid-Holocene (Fig. 5;
559 Marsicek et al., 2018), as does a speleothem-based winter temperature reconstruction
560 from Eurasia (Baker et al., 2017). These reconstructions are dominated by sites proximal
561 to the continental ice sheets, within the influence of northerly winds induced by
562 anticyclonic circulation over the ice sheet (Clark et al., 1999), or in the path of
563 downstream atmospheric flow (Baker et al., 2017). We conclude that the pattern of
564 temperature change in Arctic Alaska, including mild winter-spring temperatures in the
565 early Holocene and pronounced warming after the EMHT, was primarily forced by
566 winter-spring insolation and GHG forcing with minimal influences from ice sheet retreat
567 despite its prominent role at other northern mid-latitude sites.
568

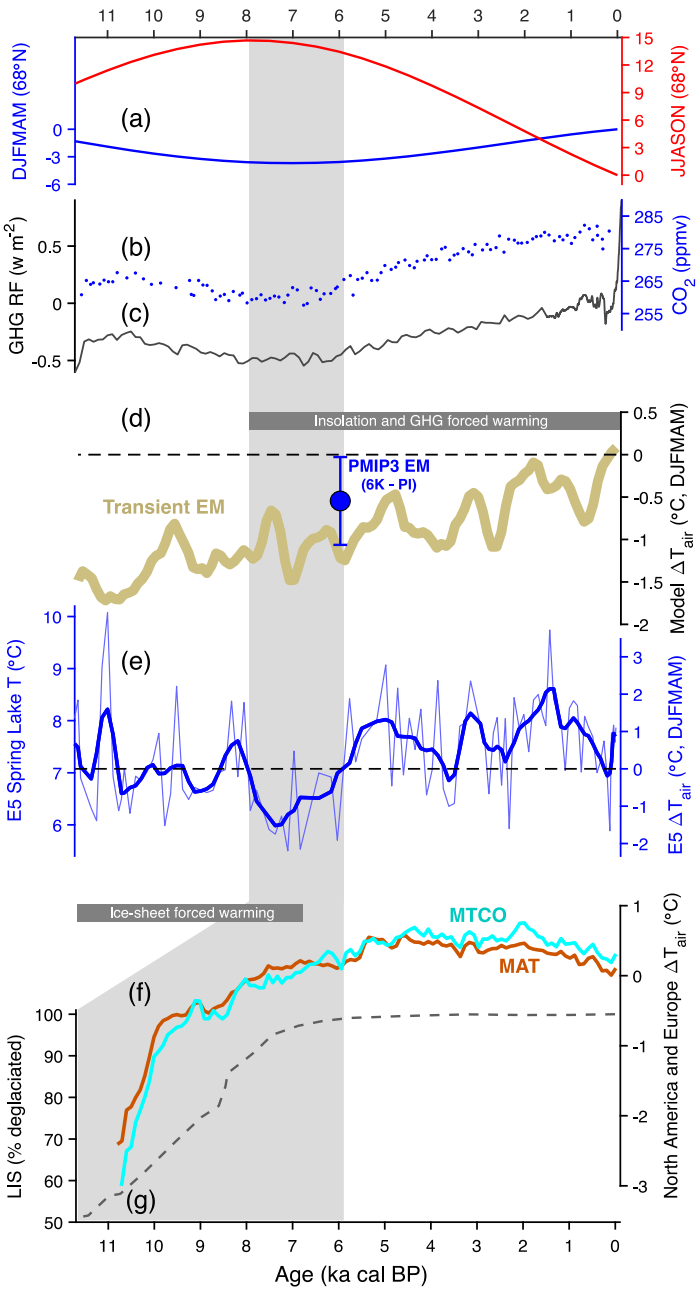

Fig. 5. Holocene cold season temperature in the context of climate forcings. (a) Mean insolation (W m^{-2}, 68 °N) for the half year corresponding to the alkenone proxy (DJFMAM) and the opposing half year (JJASON). **(b)** CO_2 concentrations recorded in Antarctic Ice (Monnin et al., 2001). **(c)** GHG radiative forcing from CO_2, CH_4, and NO_2 relative to the PI (Joos and Spahni, 2007). **(d)** GCM simulated cold season temperature anomalies (vs. PI) at Lake E5 from the 6 ka PMIP3 ensemble mean (blue dot), and the transient ensemble mean (gold). **(e)** Alkenone-inferred spring lake temperature (left axis) used to estimate DJFMAM air temperature anomalies (vs. PI) at Lake E5 (right axis). **(f)** Pollen proxy synthesis of mean annual temperature (MAT) and mean temperature of the coldest month (MTCO) from North America and Europe (Marsicek et al., 2018). **(g)** Time series of LIS deglaciation (Dyke, 2004). Gray shading indicates the Holocene temperature minimum at Lake E5 **(d,e)**, which aligns with minima in DJFMAM insolation and GHG forcing **(a-c)**. For the pollen synthesis, the Gray shading expands **(f)** to include the entire early Holocene, which was cool at mid-latitudes in North America and Eurasia in response to LIS retreat **(g)**.

Given that orbital forcing during the summer and fall (JJASON) represents a larger opposing forcing (15 w m^{-2}) than the combination of winter-spring (DJFMAM) insolation and GHG forcing (4 w m^{-2}) over the last 7 ka, it is crucial to assess whether the mean annual temperature (MAT) trend could have still been dominated by warming. Our reconstruction suggests that it was, with Holocene winter-spring warming at Lake E5 (1.4

575 – 2.2 °C) featuring a greater amplitude than the opposing summer cooling (~ 0.5 – 1 °C)
576 seen in a synthesis of terrestrial records from Alaska (Kaufman et al., 2016) and in a
577 recent summer temperature reconstruction from the Yukon based on precipitation
578 isotopes in syngenetic permafrost (Porter et al., 2019). GCM output generally support this
579 conclusion as PMIP3 simulations suggest MATs at 6 ka did not exceed PI temperatures
580 (Fig. 2). Indeed, new analysis of 6 ka climate simulations from the next phase of the
581 Proxy Model Intercomparison Project (PMIP4), which improves upon PMIP3 by
582 including realistic 6 ka GHG concentrations, shows more pronounced cooling at 6 ka vs.
583 the PI for most parts of the world, including Alaska (Brierley et al., in review, 2020).
584 Transient model simulations are more equivocal on whether mean annual temperature
585 warmed or cooled in Alaska through the Holocene; two models (CCSM3 and
586 LOVECLIM) indicate slight cooling in MAT while one model (FAMOUS) shows strong
587 warming in MAT.
588
589 *4.4. Regional Holocene Climate and Millennial-Scale Changes*
590
591 Terrestrial temperature records from Alaska and Yukon (Eastern Beringia) have primarily
592 been interpreted to represent summer temperature changes. Quantitative midge-based
593 summer temperature reconstructions suggest significant spatiotemporal temperature
594 variability in the region, with some records showing early Holocene summer warmth
595 (e.g. Kurek et al., 2009), while others suggest stable Holocene temperatures (Irvine et al.,
596 2012). South-central Alaska differs further with midge reconstructions indicating non-
597 linear responses to orbital forcing and a mid-Holocene thermal maximum (e.g. Clegg et

al., 2011). Pollen records have been used to reconstruct summer, winter and mean annual temperatures quantitatively through the Modern Analog Technique (Viau et al. 2008). However, these reconstructions may be compromised by non-analog pollen assemblages and broad ranges for key species in the transfer functions (Birks et al., 2011). Indeed, the quantitative pollen reconstructions are often at odds with qualitative pollen interpretations from the region (Viau et al., 2008). Taken at face-value, pollen reconstructions of summer temperature also suggest a mid-Holocene thermal maximum. Futhermore when pollen, midge and other geochemical records are combined into an Eastern Beringia composite, they suggest very little temperature change over the Holocene (<1 °C) due to the averaging out of spatiotemporal variations, but generally indicate a mid-Holocene thermal maximum roughly aligned with summer insolation forcing (Fig. 6b; Kaufman et al., 2016). Although this composite includes a limited number of marine records and records representing the cold seasons, it is dominated by records interpreted to reflect summer temperature over land.

In contrast to the summer- and terrestrial-dominated composite (Kaufman et al., 2016), marine records from the North Pacific and Arctic Ocean show more correspondence with winter-spring temperature changes at Lake E5. The 8 – 6 ka cal BP temperature minimum and subsequent warming trend at Lake E5 is captured in regional sea surface temperature (SST) records from the Chukchi Sea, Bering Sea and Gulf of Alaska (Fig. 6; McKay et al., 2008; Harada et al., 2014; Praetorius and Mix et al., 2014; locations shown in Fig. 1). Notably, these records were interpreted to reflect either mean annual or summer SST, but were likely sensitive to winter climate dynamics governing sea level

621 pressure and surface ocean and atmospheric circulation in the North Pacific (Trenberth
622 and Hurell, 1994). Additionally, sea ice reconstructions from the Beaufort and Chukchi
623 Seas broadly indicate periods of reduced sea ice after 6 ka cal BP (Fig. 7; McKay et al.,
624 2008; de Vernal et al., 2013; locations shown in Fig. 1). Ice in the Bering Sea forms
625 during the winter months and is sensitive to winter-spring climate dynamics affecting ice
626 formation and advection (Zhang et al., 2010). Bering Sea ice generally decreased after
627 7.5 ka cal BP (Fig. 6; Katsuki et al., 2009, Harada et al., 2014), consistent with post-
628 EMHT winter-spring warming. While sea ice concentrations likely responded to the same
629 GHG forcing and winter-spring orbital forcing trends as our proxy record, they also
630 impact terrestrial winter temperature and lake ice dynamics in northern Alaska (Alexeev
631 et al., 2016) and therefore potentially amplified spring lake temperature changes. Overall,
632 the agreement between these marine sites and the Lake E5 record demonstrates a
633 coherent regional pattern of Holocene winter-spring temperature evolution driven by
634 radiative forcing and potentially amplified by Northern Pacific atmosphere-ocean
635 dynamics and sea ice feedbacks.
636
637 Although the sea ice records in the Chukchi and Bering Seas indicate reduced ice cover
638 in the mid- to late Holocene, reconstructions from other regions within the Arctic Ocean
639 and Nordic Seas demonstrate opposite features and trends (de Vernal et al., 2013). For
640 example, ice cover expanded during the early Holocene in the Laptev Sea and maintained
641 high levels through the middle and late Holocene (Fahl and Stein, 2012). Multiproxy
642 records from the northern margin of Iceland indicate that sea ice export from the Arctic
643 Ocean through the Fram Strait steadily increased through the mid-Holocene in step with

644 neoglaciation (Moros et al., 2006; Cabedo-Sanz et al., 2016). Together, the available sea
645 ice records from the Arctic Ocean and adjacent seas suggest sea ice dynamics had unique
646 regional patterns during the Holocene, likely in response to shifts in coupled atmosphere-
647 ocean circulation patterns and relative changes in Fram Strait and Bering Strait
648 throughflow (Darby et al., 2012; de Vernal et al., 2013). Therefore, Bering and Chukchi
649 sea ice impacts on winter-spring temperature trends at Lake E5 were most likely regional
650 in nature and may have been mitigated to some extent by differing pan-arctic sea ice
651 trends during the Holocene.
652
653 In addition to the long-term Holocene trends, multi-centennial to millennial variability
654 was a prominent feature of the Lake E5 record. Winter-spring temperatures show
655 prominent local maxima centered on 5.2 and 1.4 ka cal BP (Fig. 6), with smaller events
656 visible at 11, 9.5, 8.3 and 3.2 ka cal BP. Sea ice extent and sea ice drift reconstructions
657 suggest that millennial-scale variability was a feature of Holocene climate in the
658 Beaufort, and Chukchi Seas (Darby et al., 2012; de Vernal et al., 2013). Climate
659 variability associated with changes in the strength and position of the Aleutian Low (AL)
660 is broadly present in moisture sensitive records from southern Alaska (Anderson et al.,
661 2005; Fisher et al., 2008; Kaufman et al., 2016) and has been shown to influence winter
662 climate into interior Alaska (Clegg et al., 2010). While the direct impacts of the AL on
663 Alaskan terrestrial climate are spatially complex (Anderson et al., 2015; Kaufman et al.,
664 2016) there are several lines of evidence that the AL drove millennial-scale climate
665 changes in Alaska (Kaufman et al., 2016). We suggest that millennial-scale winter-spring
666 temperature oscillations in our reconstruction from Lake E5 were driven by a

667 combination of ocean-atmosphere dynamics associated with the Aleutian Low, and
668 Arctic Ocean circulation changes controlling sea ice dynamics. Solar activity has been
669 linked to higher frequency variability in the region (Hu et al., 2003) and indeed the
670 general trend of increasing total solar irradiance from 8 to 4 ka cal BP (Steinhilber et al.,
671 2012) is in agreement with winter-spring warming at Lake E5. However, higher
672 frequency oscillations in total solar irradiance generally did not correlate with those in the
673 Lake E5 record.
674
675 The most pronounced of the submillennial-scale changes observed during the Holocene
676 at Lake E5 was a rapid warming of 1.6 ± 0.6 °C around 5.8 ka cal BP (Table S2) that
677 culminated in the temperature maxima at 5.2 ka cal BP. The event was recorded
678 regionally in records of Chukchi Sea ice extent, Bering Strait through-flow and Gulf of
679 Alaska SST (Fig. 6; McKay et al., 2008; Ortiz et al., 2009; Praetorius et al., 2015; Polyak
680 et al., 2016). It is also a prominent feature of North American and European climate and
681 aligns with mid-Holocene global change (Marsicek et al., 2019). Thus, millennial-scale
682 variability in cold season temperatures at Lake E5 likely had both regional and global
683 origins.
684

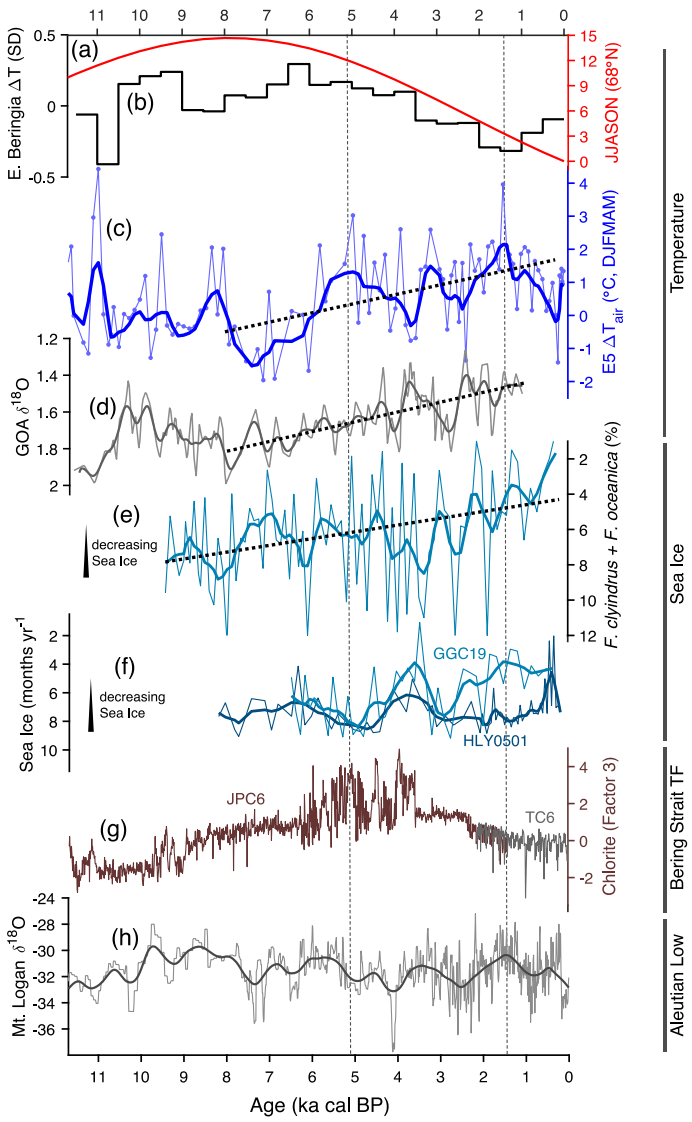

Fig. 6. Holocene climate in Eastern Beringia. (a) Mean insolation (W m^{-2}, 68 °N) for the summer and fall (JJASON). **(b)** Composite of normalized summer and/or mean annual temperature reconstructions from Eastern Beringia (Kaufman et al., 2016). **(c)** Alkenone-inferred DJFMAM air temperature at Lake E5 shown as anomalies (vs. PI) and with 8 ka – PI trend. **(d)** Gulf of Alaska $\delta^{18}O$ records from planktonic foraminifera interpreted as an indicator of mean annual SST (Praetorius and Mix, 2014). The record is shown with LOWESS smoothing and the post-EMHT trend. **(e)** Relative abundance of sea ice diatoms in core MR06-04-GC33 from the Bering Sea show with whole-record trend (Katsuki et al., 2009; Harada et al., 2014). **(f)** Dinocyst-based reconstructions of annual sea ice duration from Chuckchi Sea cores (McKay et al., 2008; de Vernal et al., 2013). **(g)** Proxy for Bering Strait throughflow based on chlorite transport to the Chukchi Sea from the North Pacific (Ortiz et al., 2009). **(h)**. Mt. Logan ice core $\delta^{18}O$ (Fisher et al., 2008). Vertical dotted lines highlight two millennial-scale winter-spring warm periods at Lake E5, which align with strengthened Bering strait throughflow and reduced Chukchi sea ice and Aleutian Low shifts, respectively.

685

686

5. Conclusions

This study provides the first quantitative alkenone-based reconstruction of Late Glacial and Holocene spring lake temperature change from Arctic Eastern Beringia. Our 16,000-year reconstruction from Lake E5 documents a series of rapid deglacial warming events that align with glacial retreat and paleo-ecological change in the region. Abrupt deglacial warming gave way to mild temperatures in the early Holocene and a long-term winter-spring warming trend. This trend occurred throughout the entire Holocene, but accelerated after 8 ka cal BP, corroborating surface temperature trends inferred from GCMs.

Our reconstruction supports the hypothesis that a warm season bias exists in regional and global proxy syntheses. Despite larger seasonal forcing from northern hemisphere summer insolation, winter-spring temperatures warmed considerably during the Holocene, balancing or exceeding summer cooling seen in a regional proxy synthesis from Eastern Beringia (Kaufman et al., 2016). Cold season temperature changes in our record, including early Holocene mild cooling followed by progressive warming since ~ 8 ka cal BP, mimic the pattern of change in GHG radiative forcing and cold season insolation, highlighting these factors, rather than ice sheet retreat, as the dominant climate drivers.

Acknowledgements

This work was funded by NSF grants PLR-1503846 to Y. Huang and J. Russell, PLR-1504069 to C. Morrill, and DEB-1637459 to E. Rastetter. Funding was also provided by a National Geographic Society Exploration Grant 9397-13 to Y. Huang, and a National Ocean Sciences Accelerator Mass Spectroscopy Internship to W. Longo. The project was greatly aided by logistical support from Toolik Field Station and limnological monitoring from the Arctic Long Term Ecological Research program (DEB-1637459). We thank X. Wang, P. Holland-Stergar and R. Tarozo for laboratory assistance. We acknowledge the World Climate Research Programme's Working Group on Coupled Modeling and the Paleoclimate Modelling Intercomparison Project for CMIP/PMIP model output. We thank two anonymous reviewers for feedback that significantly improved the manuscript.

Competing Financial Interests

The authors declare no competing financial interests.

Data Availability

Data presented in this manuscript are archived and publicly available at the National Science Foundation Arctic Data Center (doi:10.18739/A2CN6XZ7H).

References

Abbott, M.B., Edwards, M.E., Finney, B.P., 2010. A 40,000-yr record of environmental change from Burial Lake in Northwest Alaska. Quat. Res. 74, 156–165.

Alexeev, V.A., Arp, C.D., Jones, B.M., Cai, L., 2016. Arctic sea ice decline contributes to thinning lake ice trend in northern Alaska. Environ. Res. Lett. 11, 074022.

Anderson, L., Abbott, M.B., Finney, B.P., Burns, S.J., 2005. Regional atmospheric circulation change in the North Pacific during the Holocene inferred from lacustrine carbonate oxygen isotopes, Yukon Territory, Canada. Quat. Res. 64, 21–35.

Anderson, L., Berkelhammer, M., Barron, J.A., Steinman, B.A., Finney, B.P., Abbott, M.B., 2016. Lake oxygen isotopes as recorders of North American Rocky Mountain hydroclimate: Holocene patterns and variability at multi-decadal to millennial time scales. Glob. Planet. Change 137, 131–148.

Anderson, P.M., Brubaker, L.B., 1994. Vegetation history of northcentral Alaska: A mapped summary of late-quaternary pollen data. Quat. Sci. Rev. 13, 71–92.

ARC LTER database, 2016. Available from <http://ecosystems.mbl. edu/ARC/datacatalog.html>.

Arp, C.D., Jones, B.M., Grosse, G., 2013. Recent lake ice-out phenology within and among lake districts of Alaska, U.S.A. Limnol. Oceanogr. 58, 2013–2028.

Assel, R.A., Robertson, D.M., 1995. Changes in winter air temperatures near Lake Michigan, 1851-1993, as determined from regional lake-ice records. Limonology Oceanogr. 40, 165–176.

Baker, J.L., Lachniet, M.S., Chervyatsova, O., Asmerom, Y., Polyak, V.J., 2017. Holocene warming in western continental Eurasia driven by glacial retreat and greenhouse forcing. Nat. Geosci. 10.

Bartlein, P.J., Harrison, S.P., Brewer, S., Connor, S., Davis, B.A.S., Gajewski, K., Guiot, J., Harrison-Prentice, T.I., Henderson, A., Peyron, O., Prentice, I.C., Scholze, M., Seppä, H., Shuman, B., Sugita, S., Thompson, R.S., Viau, A.E., Williams, J., Wu, H., 2011. Pollen-based continental climate reconstructions at 6 and 21 ka: A global synthesis. Clim. Dyn. 37, 775–802.

Birks, H.J.B., Heiri, O., Seppä, H., Bjune, A.E., 2011. Strengths and weaknesses of quantitative climate reconstructions based on late-Quaternary biological proxies. Open Ecol. J. 3, 68–110.

Braconnot, P., Harrison, S.P., Kageyama, M., Bartlein, P.J., Masson-Delmotte, V., Abe-Ouchi, A., Otto-Bliesner, B., Zhao, Y., 2012. Evaluation of climate models using palaeoclimatic data. Nat. Clim. Chang. 2, 417–424.

Bradley, R.S., England, J.H., 2008. The Younger Dryas and the Sea of Ancient Ice. Quat. Res. 70, 1–10.

Brassell, S.C., Eglinton, G., Marlowe, I.T., Pflaumann, U., Sarnthein, M., 1986. Molecular stratigraphy: a new tool for climatic assessment. Nature 320, 129–133.

Brierley et al. (in review, 2020) Large-scale features and evaluation of the PMIP4-CMIP6 midHolocene simulations. Clim. Past Discuss., 10.5194/cp-2019-168

Cabedo-Sanz, P., Belt, S.T., Jennings, A.E., Andrews, J.T. and Geirsdóttir, Á., 2016. Variability in drift ice export from the Arctic Ocean to the North Icelandic Shelf over the last 8000 years: a multi-proxy evaluation. Quat. Sci. Rev. 146, 99-115.

Caissie, B.E., Brigham-Grette, J., Lawrence, K.T., Herbert, T.D., Cook, M.S., 2010. Last

Glacial Maximum to Holocene sea surface conditions at Umnak Plateau, Bering Sea, as inferred from diatom, alkenone, and stable isotope records. Paleoceanography 25, PA1206.
Clark, P.U., Alley, R.B., Pollard, D., 1999. Northern Hemisphere Ice-Sheet Influences on Global Climate Change. Science (80-.). 286, 1104–1112.
Clegg, B.F., Hu, F.S., 2010. An oxygen-isotope record of Holocene climate change in the south-central Brooks Range, Alaska. Quat. Sci. Rev. 29, 928–939.
Clegg, B.F., Kelly, R., Clarke, G.H., Walker, I.R., Sheng, F., 2011. Nonlinear response of summer temperature to Holocene insolation forcing in Alaska Proc. Natl. Acad. Sci. U. S. A. 108, 19299–19304.
Conte, M.H., Sicre, M.-A., Rühlemann, C., Weber, J.C., Schulte, S., Schulz-Bull, D., Blanz, T., 2006. Global temperature calibration of the alkenone unsaturation index (UK′37) in surface waters and comparison with surface sediments. Geochemistry, Geophys. Geosystems 7, 10.1029/2005GC001054.
D'Andrea, W.J., Huang, Y., Fritz, S.C., Anderson, N.J., 2011. Abrupt Holocene climate change as an important factor for human migration in West Greenland. Proc. Natl. Acad. Sci. U. S. A. 108, 9765–9.
D'Andrea, W.J., Lage, M., Martiny, J.B.H., Laatsch, A.D., Amaral-Zettler, L. a., Sogin, M.L., Huang, Y., 2006. Alkenone producers inferred from well-preserved 18S rDNA in Greenland lake sediments. J. Geophys. Res. 111, G03013.
D'Andrea, W.J., Theroux, S., Bradley, R.S., Huang, X., 2016. Does phylogeny control UK37-temperature sensitivity? Implications for lacustrine alkenone paleothermometry. Geochim. Cosmochim. Acta 175, 168–180.
Darby, D.A., Ortiz, J.D., Grosch, C.E., Lund, S.P., 2012. 1,500-year cycle in the Arctic Oscillation identified in Holocene Arctic sea-ice drift. Nat. Geosci. 5, 897–900.
de Vernal, A., Hillaire-marcel, C., Rochon, A., Fréchette, B., Henry, M., Solignac, S., Bonnet, S., 2013. Dinocyst-based reconstructions of sea ice cover concentration during the Holocene in the Arctic Ocean, the northern North Atlantic Ocean and its adjacent seas. Quat. Sci. Rev. 79, 111–121.
Dee, S.G., Russell, J.M., Morrill, C., Chen, Z., Neary, A., 2018. PRYSM v2 . 0 : A Proxy System Model for Lacustrine Archives. Paleoceanogr. Paleoclimatology.
Denton, G.H., Alley, R.B., Comer, G.C., Broecker, W.S., 2005. The role of seasonality in abrupt climate change. Quat. Sci. Rev. 24, 1159–1182.
Déry, S.J., Stieglitz, M., Rennermalm, Å.K., Wood, E.F., 2005. The Water Budget of the Kuparuk River Basin, Alaska. J. Hydrometeorol. 6, 633–655.
Dyke, A.S., 2004. An outline of North American deglaciation with emphasis on central and northern Canada, in: Ehlers, J., Gibbard, P. (Eds.), Developments in Quaternary Sciences. Elsevier B.V., pp. 373–424.
Eisner, W.R., Colinvaux, P.A., 1992. Late Quaternary Pollen Records from Oil Lake and Feniak Alaska, U.S.A. Arct. Alp. Res. 24, 56–63.
Environmental Data Center Team. 2016. Meteorological monitoring program at Toolik, Alaska. Toolik Field Station, Institute of Arctic Biology, University of Alaska Fairbanks, Fairbanks, AK 99775.
http://toolik.alaska.edu/edc/abiotic_monitoring/data_query.php
Fahl, K. and Stein, R., 2012. Modern seasonal variability and deglacial/Holocene change

of central Arctic Ocean sea-ice cover: New insights from biomarker proxy records. Earth Planet. Sci. Lett. 351, pp.123-133.
Fisher, D., Osterberg, E., Dyke, A., Dahl-jensen, D., Demuth, M., Zdanowicz, C., Bourgeois, J., Roy, M., Mayewski, P., Wake, C., Kreutz, K., Zheng, J., Yalcin, K., Goto-azuma, K., Rupper, S., 2008. The Mt Logan Holocene – late Wisconsinan isotope record : tropical Pacific – Yukon connections 5, 667–677.
Foley, J.A., Kutzbach, J.E., Coe, M.T., Levis, S., 1994. Feedbacks between climate and boreal forests during the Holocene epoch. Nature 371, 52–54.
Gaglioti, B. V, Mann, D.H., Wooller, M.J., Jones, B.M., Wiles, G.C., Groves, P., Kunz, M.L., Baughman, C.A., Reanier, R.E., 2017. Younger-Dryas cooling and sea-ice feedbacks were prominent features of the Pleistocene-Holocene transition in Arctic Alaska. Quat. Sci. Rev. 169, 330–343.
Hamilton, T.D., 1982. A late Pleistocene glacial chronology for the southern Brooks Range: Stratigraphic record and regional significance. Geol. Soc. Am. Bull. 93, 700–716.
Harada, N., Katsuki, K., Nakagawa, M., Matsumoto, A., Seki, O., Addison, J. a., Finney, B.P., Sato, M., 2014. Holocene sea surface temperature and sea ice extent in the Okhotsk and Bering Seas. Prog. Oceanogr. 126, 242–253.
Hu, F.S., Kaufman, D., Yoneji, S., Nelson, D., Shemesh, A., Huang, Y., Tian, J., Bond, G., Clegg, B. and Brown, T., 2003. Cyclic variation and solar forcing of Holocene climate in the Alaskan subarctic. Science 301(5641), 1890-1893.
Huryn, A. and Hobbie, J., 2012. Land of extremes: a natural history of the Arctic North Slope of Alaska. University of Alaska Press.
Hostetler, S., Bartlein, P., 1990. Simulation of Lake Evaporation with Application to Modeling Lake Level Variations, Oregon. Water Resour. Res. 26, 2603–2612.
Irvine, F., Cwynar, L.C., Vermaire, J.C., Rees, A.B.H., 2012. Midge-inferred temperature reconstructions and vegetation change over the last ~15,000 years from Trout Lake, northern Yukon Territory, eastern Beringia. J. Paleolimnol. 48, 133–146.
Joos, F., Spahni, R., 2008. Rates of change in natural and anthropogenic radiative forcing over the past 20,000 years. Proc. Natl. Acad. Sci. 105, 1425–1430.
Katsuki, K., Khim, B.-K., Itaki, T., Harada, N., Sakai, H., Ikeda, T., Takahashi, K., Okazaki, Y., Asahi, H., 2009. Land-sea linkage of Holocene paleoclimate on the Southern Bering Continental Shelf. The Holocene 19, 747–756.
Kaufman, D., 2004. Holocene thermal maximum in the western Arctic (0–180°W). Quat. Sci. Rev. 23, 529–560.
Kaufman, D.S., Axford, Y.L., Henderson, A.C.G., McKay, N.P., Oswald, W.W., Saenger, C., Anderson, R.S., Bailey, H.L., Clegg, B., Gajewski, K., Hu, F.S., Jones, M.C., Massa, C., Routson, C.C., Werner, A., Wooller, M.J., Yu, Z., 2016. Holocene climate changes in eastern Beringia (NW North America) – A systematic review of multi-proxy evidence. Quat. Sci. Rev. 147, 312–339.
Kaufman, D.S., Schneider, D.P., McKay, N.P., Ammann, C.M., Bradley, R.S., Briffa, K.R., Miller, G.H., Otto-Bliesner, B.L., Overpeck, J.T., Vinther, B.M., 2009. Recent warming reverses long-term arctic cooling. Science 325, 1236–9.
Kokorowski, H.D., Anderson, P.M., Mock, C.J., Lozhkin, A. V., 2008. A re-evaluation and spatial analysis of evidence for a Younger Dryas climatic reversal in Beringia. Quat. Sci. Rev. 27, 1710–1722.

862 Kurek, J., Cwynar, L.C., Ager, T.A., Abbott, M.B., Edwards, M.E., 2009. Late
863 Quaternary paleoclimate of western Alaska inferred from fossil chironomids and its
864 relation to vegetation histories. Quat. Sci. Rev. 28, 799–811.
865 Laskar, J., Robutel, P., Joutel, F., Gastineau, M., Correia, a. C.M., Levrard, B., 2004. A
866 long-term numerical solution for the insolation quantities of the Earth. Astron.
867 Astrophys. 428, 261–285.
868 Liu, Z., He, F., Brady, E.C., Tomas, R., Clark, P.U., Carlson, A.E., Curry, W., Brook, E.,
869 Erickson, D., Jacob, R., Kutzbach, J., Cheng, J., 2009. Transient Simulation of Last
870 Deglaciation with a New Mechanism for Bølling-Allerød Warming. Science (80-.).
871 413, 310–315.
872 Liu, Z., Zhu, J., Rosenthal, Y., Zhang, X., Otto-Bliesner, B.L., Timmermann, A., Smith,
873 R.S., Lohmann, G., Zheng, W., Timm, O.E., 2014. The Holocene temperature
874 conundrum. Proc. Natl. Acad. Sci. 111, E3501--E3505.
875 Livingstone, D.M., 1997. Break-up dates of Alpine lakes as proxy data for local and
876 regional mean surface air temperatures. Clim. Change 37, 407–439.
877 Longo, W.M., Dillon, J.T., Tarozo, R., Salacup, J.M., Huang, Y., 2013. Unprecedented
878 separation of long chain alkenones from gas chromatography with a
879 poly(trifluoropropylmethylsiloxane) stationary phase. Org. Geochem. 65, 94–102.
880 Longo, W.M., Huang, Y., Yao, Y., Zhao, J., Giblin, A.E., Wang, X., Zech, R., Haberzettl,
881 T., Jardillier, L., Toney, J., Liu, Z., Krivonogov, S., Kolpakova, M., Chu, G.,
882 D'Andrea, W.J., Harada, N., Nagashima, K., Sato, M., Yonenobu, H., Yamada, K.,
883 Gotanda, K., Shinozuka, Y., 2018. Widespread occurrence of distinct alkenones
884 from Group I haptophytes in freshwater lakes: Implications for paleotemperature
885 and paleoenvironmental reconstructions. Earth Planet. Sci. Lett. 492, 239–250.
886 Longo, W.M., Theroux, S., Giblin, A.E., Zheng, Y., James, T., Huang, Y., Longo, W.M.,
887 Theroux, S., Giblin, A.E., Zheng, Y., Dillon, J.T., Huang, Y., 2016. Temperature
888 calibration and phylogenetically distinct distributions for freshwater alkenones:
889 Evidence from northern Alaskan lakes. Geochim. Cosmochim. Acta 180, 177–196.
890 Magnuson, J.J., Robertson, D.M., Benson, B.B., Wynne, R.H., Livingstone, D.M., Arai,
891 T., Assel, R.A., Barry, R.G., Card, V., Kuusisto, E., Granin, N.G., Prowse, T.,
892 Stewart, K.M., Vuglinski, V.S., 2000. Historical Trends in Lake and River Ice Cover
893 in the Northern Hemisphere. Science (80-.). 289, 1743–1746.
894 Manley, W.F., 2002. Postglacial flooding of the bering land Bridge: a geospatial
895 animation v1. INSTAAR. WWW Document. http://instaar.colorado.edu/QGISL/
896 bering_land_bridgel.
897 Mann, D.H., Groves, P., Reanier, R.E., Kunz, M.L., 2010. Floodplains, permafrost,
898 cottonwood trees, and peat: What happened the last time climate warmed suddenly
899 in arctic Alaska? Quat. Sci. Rev. 29, 3812–3830.
900 Mann, D.H., Peteet, D.M., Reanier, R.E., Kunz, M.L., 2002. Responses of an arctic
901 landscape to Lateglacial and early Holocene climatic changes: the importance of
902 moisture. Quat. Sci. Rev. 21, 997–1021.
903 Marcott, S.A., Shakun, J.D., Clark, P.U., Mix, A.C., 2013. A Reconstruction of Regional
904 and Global Temperature for the Past 11,300 Years. Science 339, 1198–1201.
905 Marlowe, I.T., Green, J.C., Neal, A.C., Brassell, S.C., Eglinton, G., Course, P.A., 1984.
906 Long chain (n-C37 – C39) alkenones in the Prymnesiophyceae. Distribution of
907 alkenones and other lipids and their taxonomic significance. Br. Phycol. J. 19, 203–

908 216.
909 Marsicek, J., Shuman, B.N., Bartlein, P.J., Shafer, S.L., Brewer, S., 2018. Reconciling
910 divergent trends and millennial variations in Holocene temperatures. Nature 554,
911 92–96.
912 Mayewski, P.A., Rohling, E.E., Stager, J.C., Karl??n, W., Maasch, K.A., Meeker, L.D.,
913 Meyerson, E.A., Gasse, F., van Kreveld, S., Holmgren, K., Lee-Thorp, J., Rosqvist,
914 G., Rack, F., Staubwasser, M., Schneider, R.R., Steig, E.J., 2004. Holocene climate
915 variability. Quat. Res. 62, 243–255.
916 McKay, J.L., de Vernal, A., Hillaire-Marcel, C., Not, C., Polyak, L., Darby, D., 2008.
917 Holocene fluctuations in Arctic sea-ice cover: dinocyst-based reconstructions for the
918 eastern Chukchi Sea. Can. J. Earth Sci. 45, 1377–1397.
919 Meyer, H., Opel, T., Laepple, T., Dereviagin, A.Y., Hoffmann, K., Werner, M., 2015.
920 Long-term winter warming trend in the Siberian Arctic during the mid- to late
921 Holocene. Nat. Geosci. 8, 122–125.
922 Meyer, H., Schirrmeister, L., Yoshikawa, K., Opel, T., Wetterich, S., Hubberten, H.W.,
923 Brown, J., 2010. Permafrost evidence for severe winter cooling during the Younger
924 Dryas in northern Alaska. Geophys. Res. Lett. 37, 1–5.
925 Monnin, E., Indermühle, a, Dällenbach, a, Flückiger, J., Stauffer, B., Stocker, T.F.,
926 Raynaud, D., Barnola, J.M., 2001. Atmospheric CO2 concentrations over the last
927 glacial termination. Science 291, 112–114.
928 Moros, M., Andrews, J.T., Eberl, D.D. and Jansen, E., 2006. Holocene history of drift ice
929 in the northern North Atlantic: Evidence for different spatial and temporal modes.
930 Paleoceanogr. 21(2).
931 Opel, T., Meyer, H., Wetterich, S., Laepple, T., Dereviagin, A. and Murton, J., 2018. Ice
932 wedges as archives of winter paleoclimate: A review. Permafrost and Periglacial
933 Processes, 29(3), pp.199-209.
934 Ortiz, J.D., Polyak, L., Grebmeier, J.M., Darby, D., Eberl, D.D., Naidu, S., Nof, D., 2009.
935 Provenance of Holocene sediment on the Chukchi-Alaskan margin based on
936 combined diffuse spectral reflectance and quantitative X-Ray Diffraction analysis.
937 Glob. Planet. Change 68, 73–84.
938 Palecki, M.A., Barry, R.G., 1986. Freeze-up and Break-up of Lakes as an Index of
939 Temperature Changes during the Transition Seasons: A Case Study for Finland. J.
940 Clim. Appl. Meteorol. 25, 893–902.
941 Pendleton, S.L., Ceperley, E.G., Briner, J.P., Kaufman, D.S., Zimmerman, S., 2015.
942 Rapid and early deglaciation in the central Brooks Range, Arctic Alaska. Geology
943 43, 419–422.
944 Polyak, L., Belt, S.T., Cabedo-Sanz, P., Yamamoto, M., Park, Y.-H., 2016. Holocene sea-
945 ice conditions and circulation at the Chukchi-Alaskan margin, Arctic Ocean,
946 inferred from biomarker proxies. The Holocene 26, 1810–1821.
947 Porter, T.J., Schoenemann, S.W., Davies, L.J., Steig, E.J., Bandara, S. and Froese, D.G.,
948 2019. Recent summer warming in northwestern Canada exceeds the Holocene
949 thermal maximum. Nat. Commun. 10(1), 1-10.
950 Praetorius, S.K., Mix, A.C., 2014. Synchronization of North Pacific and Greenland
951 climates preceded abrupt deglacial warming. Science (80-.). 345, 444–448.
952 Praetorius, S.K., Mix, A.C., Walczak, M.H., Wolhowe, M.D., Addison, J.A., Prahl, F.G.,
953 2015. North Pacific deglacial hypoxic events linked to abrupt ocean warming.

Nature 527, 362–366.
Richter, N., Longo, W.M., George, S., Shipunova, A., Huang, Y., Amaral-Zettler, L., 2019. Phylogenetic diversity in freshwater-dwelling Isochrysidales haptophytes with implications for alkenone production. Geobiology 17, 272–280.
Shah Walter, S.R., Gagnon, A.R., Roberts, M.L., McNichol, A.P., Lardie Gaylord, M.C., Klein, E., 2015. Ultra-small graphitization reactors for ultra-microscale 14C analysis at the National Ocean Sciences Accelerator Mass Spectrometry (NOSAMS) facility. Radiocarbon 57, 109–122.
Smith, R.S., Gregory, J., 2012. The last glacial cycle: transient simulations with an AOGCM. Clim. Dyn. 38, 1545–1559.
SNOTEL site 968, 2016. Snow Telemetry Data Collection Network, Snow Survey and Water Supply Forecasting Program, National Water and Climate Center, United States Department of Agriculture. https://wcc.sc.egov.usda.gov/nwcc/site?sitenum=968
Stager, J.C., Mayewski, P.A., 1997. Abrupt Early to Mid-Holocene Climatic Transition Registered at the Equator and the Poles. Science (80-.). 276, 1834–1836.
Steinhilber, F., Abreu, J.A., Beer, J., Brunner, I., Christl, M., Fischer, H., Heikkilä, U., Kubik, P.W., Mann, M., McCracken, K.G. and Miller, H., 2012. 9,400 years of cosmic radiation and solar activity from ice cores and tree rings. Proc. Natl. Acad. Sci. U. S. A. 109(16), 5967-5971.
Sundqvist, H.S., Kaufman, D.S., McKay, N.P., Balascio, N.L., Briner, J.P., Cwynar, L.C., Sejrup, H.P., Seppä, H., Subetto, D.A., Andrews, J.T., Axford, Y., Bakke, J., Birks, H.J.B., Brooks, S.J., de Vernal, A., Jennings, A.E., Ljungqvist, F.C., Rühland, K.M., Saenger, C., Smol, J.P., Viau, A.E., 2014. Arctic Holocene proxy climate database - new approaches to assessing geochronological accuracy and encoding climate variables. Clim. Past 10, 1605–1631.
Timm, O.E., Timmermann, A., 2007. Simulation of the Last 21 000 Years Using Accelerated Transient Boundary Conditions. J. Clim. 20, 4377–4401.
Trenberth, K.E., Hurrell, J.W., 1994. Decadal atmosphere-ocean variations in the Pacific. Clim. Dyn. 9, 303–319.
Vachula, R.S., Huang, Y., Longo, W.M., Dee, S.G., Daniels, W.C., Russell, J.M., 2019. Evidence of Ice Age humans in eastern Beringia suggests early migration to North America. Quat. Sci. Rev.
Viau, A.E., Gajewski, K., Sawada, M.C., Bunbury, J., 2008. Low- and High-Frequncy Climate Variability in Eastern Beringia During the Past 25000 Years. Can. J. Earth Sci. 45, 1435–1453.
Volkman, J.K., Eglinton, G., Corner, E.D.S., Forsberg, T.E.V., 1980. Long-chain alkenes and alkenones in the marine coccolithophorid *Emiliania huxleyi*. Phytochemistry 19, 2619–2622.
Zhang, J., Woodgate, R. and Moritz, R., 2010. Sea ice response to atmospheric and oceanic forcing in the Bering Sea. J. Phys. Oceanogr. 40(8), 1729-1747.

996